A SCINTILLATING PROBLEM: BASIN SCALE ACOUSTIC PROPAGATION THROUGH A FLUCTUATING OCEAN.

John A. Colosi

Woods Hole Oceanographic Institution, Woods Hole Massachusetts 02543,
jcolosi@whoi.edu

1. ABSTRACT

Basin scale acoustic propagation through the fluctuating ocean is a fascinating problem in stochastic wave propagation because of the "magnification" of scattering effects over such long ranges. Indeed, based on a decade of observations in the 1990's it has been found that there are serious shortcomings in the standard theory of ocean acoustic wave propagation in random media, where the primary scattering is due to internal gravity waves. The standard theory comes from a perturbation expansion about the deterministic ray using Feyman path integral techniques. New theoretical approaches involve application of the notions of ray chaos and broadband scattering as well as the consideration of ocean scattering by mesoscale turbulence and other small-scale processes. In honour of receiving the A.B. Wood award, this review of basin scale acoustic propagation is dedicated to Albert B. Wood whose wonderful curiosity and basic physics approach to ocean acoustics and naval science is an inspiration to us all.

KEY WORDS: Waves in Random Media; Basin Scale Acoustics

2. INTRODUCTION

Albert B. Wood was a renaissance scientist who combined many areas of knowledge into his work on underwater acoustics and naval science, including engineering (mechanical, electrical or ocean), biology, geology, chemistry, and his area of training, physics. He made fundamental contributions to the areas of sonar (ASDICS as it was then called in Britain), bioacoustics and marine mammal training, low radar, sound transmission though bubbly media, geo-acoustics, and the classical problem of sound propagation in the coastal wedge. What a wonderful time it must have been for him to have participated in the genesis of so many fields of study! We are no less fortunate today with many exciting new areas of discovery still open. I have no doubt that A. B. Wood would be fascinated by the notion that the ocean sound channel can transmit sound over ocean basins (and between basins!) with surprising fidelity, and that that sound can be used to make unique measurements of ocean thermal structure and dynamics. This review of basin scale acoustics is dedicated to A.B. Wood in my appreciation of receiving the Institute of Acoustics award that bears his name.

In the 1990's, interest in basin scale acoustic propagation was fostered by Walter Munk who proposed using acoustic remote sensing techniques to measure heat content changes of the world oceans to better understand both anthropogenic changes and natural climatic variability [Munk and Forbes, 1989; Spiesberger and Metzger, 1990]. These observations of ocean heat content could be used to better evaluate the predictive skill of coupled ocean-atmosphere models and determine if those models could be trusted to make long-term (decadal to century) forecasts. While the actual spatial signature of ocean climatic variability is more complicated, a simple calculation assuming a diffusive heating from the surface of 30 $m^{\circ}C$/year with a vertical e-folding scale of 1km demonstrates that the resulting 20 ms/year travel time change over a 1000km acoustic propagation path is well within the detection range of acoustic methods, given 3-5 years

to average over ocean weather and inter-annual variability [Munk, Worcester and Wunsch, 1995; Semtner , 1990].

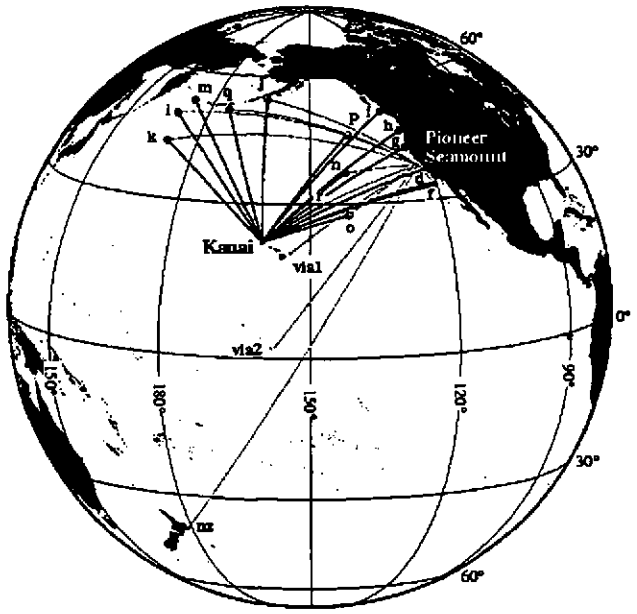

Figure 1: The ATOC North Pacific Network. Sources of 250W, 75Hz broadband sound were located on Pioneer seamount west of San Francisco, and north of Kauai. Alphabetic symbols are fictive positions of Navy SOSUS receivers and vla1 and vla2 are vertical line arrays which were briefly deployed for 8 months in 1996. The New Zealanders had a single hydrophone receiver that operated for roughly a year also in 1996.

The Acoustic Thermometry of Ocean Climate (ATOC) program was due to commence basin scale measurements in 1994 from a North Pacific network like that shown in figure 1. However, concerns over the impact of the sound sources on marine mammals significantly delayed the project. Between 1996 and 1998, and under very restrictive oversight, ATOC transmitted intermittently from a source located off San Francisco, California. Between 1998 and 2000, and under similar oversight, signals were transmitted from a source off Kauai (there was a short period in 1998 where both sources were operating). Sadly, the ATOC time series was too short and intermittent to achieve the ambitious ocean climate goals of the program, though some progress was achieved in ground-truthing satellite altimetry estimates of ocean heat content [The ATOC Group, 1998]. However, the ATOC transmissions have contributed significantly to our understanding of acoustic variability [Colosi et al. 1999a,b; Dushaw et al.,1999], and the effects of sound on marine mammals [Au, Nachtigall, and Pawlowski, 1997; Frankel, and Clark, 1998; Klimey, and Beavers, 1998; Costa et al., 1998; Frankel and Clark, 2000] . The increased understanding of acoustic variability does have positive rewards for acoustic thermometry, since acoustic variability imposes the ultimate limitations on thermometry in the same way ground based telescopes are limited by atmospheric turbulence. Future observing systems will be designed to better mitigate the now anticipated variability. In addition, the marine mammal studies have shown that there was no significant impact of the ATOC sources on marine mammals.

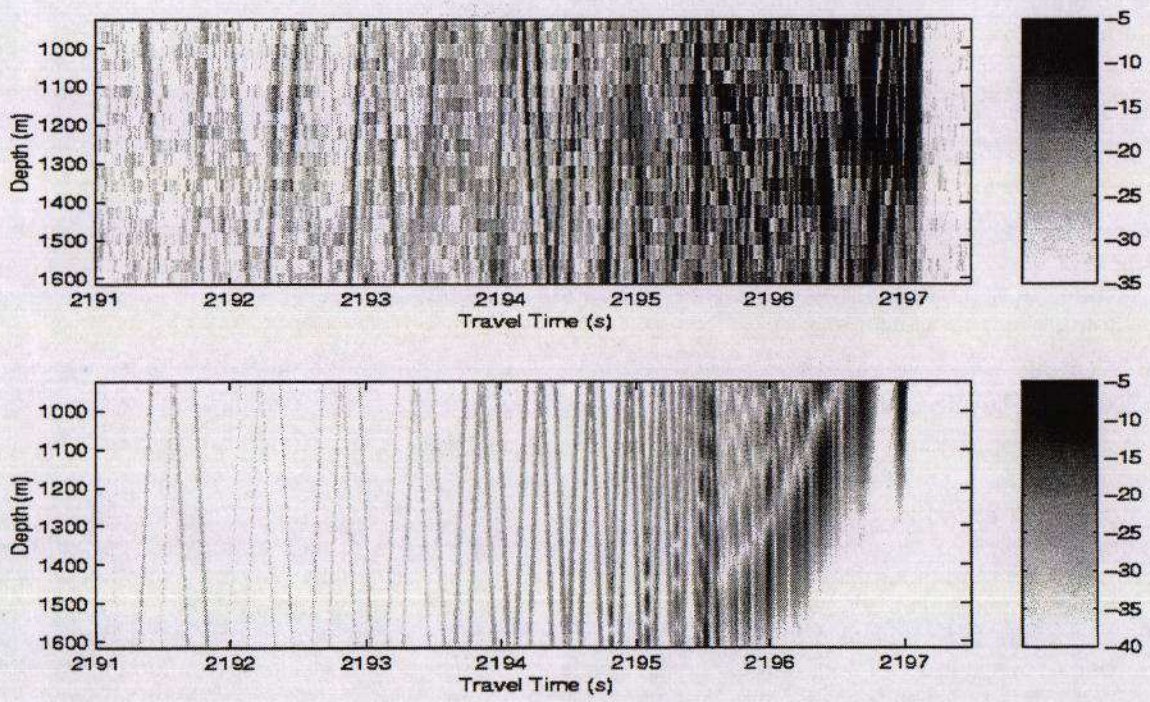

Figure 2: Measured (upper) and simulated (lower) time fronts for a 3250-km ATOC transmission originating off California to a 700-m long receiving array located off the Hawaiian Islands. The signal center frequency is 75 Hz and the bandwidth (3dB points) is 37.5 Hz. The simulation is a parabolic equation calculation using sound speed profiles derived from climatology and CTD and XBT casts taken along the transmission path. The intensity scale is in (dB) relative to the maximum intensity at the receiver.

Figure 2 shows an example of a 3250 km acoustic pulse transmission received on a 700-m long vertical line array (upper panel). The observed pulse shows two distinct regions in the arrival pattern. Acoustic energy which arrives early has the distinct wavefront pattern shown in the simulation (lower panel). This is the data of a traditional acoustic tomography analysis, since points along the wavefront can be identified with specific geometrical acoustics ray paths that sample the ocean in a specific way. In this "wavefront" region, acoustic variability is apparently rather weak and the probability density function (PDF) of peak intensity is quite close to log-normal. Also the pulse time spread is much less than the time wander. On the other hand, there is distinct wave front fracturing or multipathing, normally associated with stronger scattering, so that on average there are about 2 peaks per wavefront arm per hydrophone depth [Colosi, Tappert, and Dzieciuch; 2001]. Further, the intensity variability is a strong function of time delay relative to the peak arrival time [Colosi, Tappert, and Dzieciuch; 2001]. Interestingly, the standard theory predicts strong scattering in this region where the pulse time spread is much larger than time wander, and the PDF of intensity should be close to exponential. The wavefront region does not persist throughout the arrival pattern, and near travel time 2195 (s) the wavefront pattern is lost to a very confused pattern between times 2195 (s) and 2197(s). This transition is very abrupt, and it is found that the acoustic variability in this 2-sec "finale" region is suggestive of strong

scattering. We note also that the simulation suggests that the wavefront pattern should persist to time 2195.5 (s) or so and that there should be a strong deep shadow-zone between times 2196 (s) and 2197(s). However, the observations show no such behaviour. Further, as will be discussed subsequently, with regard to the theory neither the rapid wavefront-to-finale transition nor the filling-in of the shadow zone are predicted, and the correct prediction of strong scattering by the theory is purely fortuitous. Thus the data show many interesting and first order features that need theoretical explanation.

The general outline of this paper is as follows. In section 3 a detailed discussion of the theory/observation comparisons is given. Section 4 discusses new theoretical approaches which includes a discussion of ray chaos and of broadband scattering physics. The final section 5 has summary and conclusions.

3. COMPARISONS WITH THEORY

The basic theory of acoustic propagation through the fluctuating ocean was developed by S. M. Flatt'e, W. Munk, R. Dashen, F. Zachariasen, and co-workers and was summarized in the monograph edited by Flatt'e [1979], and later in a review by Flatt'e[1983]. Previous work in the area of waves in random media had largely been concerned with electromagnetic propagation through homogeneous isotropic turbulence advected by a mean wind (Taylors Hypothesis) with constant background wave speed. The monumental achievement of the work of Flatt'e and co-workers was to formulate a theory that simultaneously accounted for all of the novel aspects of ocean acoustic propagation, namely anisotropic and inhomogenous sound speed fluctuations, the intrinsic times dependence of the medium (internal waves with a dispersion relation), and the oceanic acoustic waveguide.

3.1 Wave Propagation Regimes: Λ, Φ Theory

The description of ocean acoustic wave propagation regimes begins with the Rytov approximation [Flatt'e et al., 1979] in which the variance of log-intensity $\sigma^2_{\ln I} = \langle \iota^2 \rangle - \langle \iota \rangle^2$ and phase $\langle \phi^2 \rangle$ are given by

$$\langle \phi^2 \rangle = q^2 \int_\Gamma ds < \mu^2 > L_p(\theta, z) G_+(R_f, k_z) \qquad (1)$$

$$\sigma^2_{\ln I} = 4q^2 \int_\Gamma ds < \mu^2 > L_p(\theta, z) G_-(R_f, k_z) \qquad (2)$$

where

$$G_{+/-}(R_f, k_z) = \frac{1}{2} \sum_{j=1}^{\infty} \frac{H(j)}{j} \left[1 \pm \cos\left(\frac{k_z^2(j) R_f^2}{2\pi} \right) \right] \qquad (3)$$

Here $q = \sigma / c_0$ is the acoustic wavenumber, Γ is the unperturbed geometrical optics ray path (i.e. no sound speed fluctuations), $\langle \mu^2(z) \rangle$ is the fractional sound speed variance, $L_p(\theta, z)$ is the

effective correlation length of the sound speed fluctuations along the ray path, and $G_{+/-}$ is the Fresnel Filter which is a function of the internal wave vertical wavenumber k_z, the vertical mode number spectrum of internal waves $H(j)$, and the Fresnel radius R_f. Two limits are of interest here: Geometrical Optics $k_z R_f << 1$, and large diffraction $k_z R_f >> 1$. If we define two new parameters,

$$\Phi^2 = q^2 \int_\Gamma ds < \mu^2 > L_p(\theta, z) \tag{4}$$

$$\Lambda = \frac{q^2}{\Phi^2} \int_\Gamma ds < \mu^2 > L_p(\theta, z) \frac{\{k_z^2\} R_f^2}{2\pi} \tag{5}$$

where the curly brackets on k_z^2 denotes a spectrum average as described in Esswein and Flatt'e, [1981], then the 2 limiting cases become:

1) Geometrical optics, $\Lambda << 1$, $\langle \phi^2 \rangle = \Phi^2$ and $\sigma_{\ln I}^2 = \pi/2 \Lambda \Phi^2$

2) Large diffraction, $\Lambda >> 1$, $\langle \phi^2 \rangle = \Phi^2/2$ and $\sigma_{\ln I}^2 = 2\Phi^2$.

These results can be used to denote wave propagation regimes, where the parameter Φ is the rms phase fluctuations computed in the geometrical optics approximation and Λ is called the diffraction parameter and measures the range average ratio of the Fresnel radius (typical acoustic field scale) to the vertical correlation length of the random medium $L_z^{-2} = \{k_z^2\}$. A condition for the onset of strong scattering is $\sigma_{\ln I}^2 \approx O(1)$. Therefore, on a plot of Φ vs Λ we have the strong scattering boundaries corresponding to conditions (1) and (2) above as $\Lambda\Phi^2=1$ and $\Phi = 1$. These boundaries are shown in figure 3. More general considerations regarding the breakup of a ray path into many independent micro-rays gives the stronger condition of $\Lambda\Phi = 1$ [Flatt'e et al, 1979], which is also shown in figure 3.

A qualitative understanding of the 3 propagation regimes depicted in figure 3 is necessary for the interpretation of basin scale acoustic fluctuations results. The unsaturated regime, for which $\Lambda < 1$ and $\Lambda\Phi^2 < 1$, is adequately described by geometrical optics in which the acoustic field from an impulsive source can be understood in terms of a ***single*** deterministic ray path modulated by the random medium. In the unsaturated regime the probability density function (PDF) for intensity is very nearly log-normal, and an initially thin transmitted pulse will remain thin. The fully saturated regime, where $\Phi > 1$ and $\Lambda\Phi > 1$, is characterized by the break-up of the deterministic ray into many uncorrelated micro-rays. Here the intensity PDF is nearly exponential (Rayleigh in amplitude), $\sigma_{\ln I}^2 \to \pi^2/6$, and an initially thin transmitted pulse becomes broadened in time since micro-rays have variable phase. For $\Lambda < 1$ with $\Lambda\Phi^2 > 1$ and $\Lambda\Phi < 1$, a third propagation regime called the partially saturated regime exisits. In this case micro-rays are created by the small scale sound speed fluctuations but they are modulated by the large scales, thus creating

correlations. In this regime pulse time spread and time wander can be of comparable sizes and $\sigma^2_{\ln I}$ attains its maximum values. Predictions are difficult to make in this regime, since the details of the micro-ray correlation are crucial.

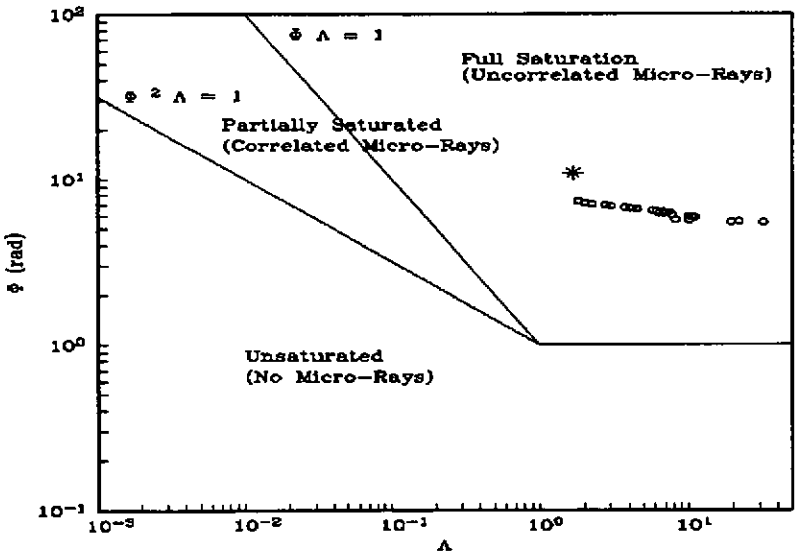

Figure 3: Λ, Φ diagram for North Eastern Pacific basin scale acoustic propagation at a range of 3250km. The unsaturated, partially saturated and fully saturated propagation regimes are identified. Predictions for the experiment are the open circles (identified wavefronts) and the star (axial cut-off). The earliest ray arrivals have the largest Λ values.

3.2 Comparison of observations and predictions

With the previous background material in hand a discussion of the comparisons between observed and predicted acoustic fluctuations can proceed. Many of these results have been presented elsewhere [Colosi et al., 1999a,b; Colosi, Tappert, and Dzieciuch, 2001]. Figure 3 shows where assorted rays fall on the Λ,Φ diagram for 3252km propagation in the north-eastern Pacific Ocean, where the sound speed fluctuations are described by the Garrett-Munk internal wave spectrum [Munk, 1981; Colosi and Brown, 1998]. All of the points fall within the fully saturated regime in which the signal is interpreted as a mutlipath interference pattern of many uncorrelated microrays.

3.2.1 The wavefront region

For the wavefront region, where individual wavefronts can be identified, several observations contradict the interpretation that the signal is an interference pattern of uncorrelated microrays. First the observed rms phase fluctuations for 1000-5000 km propagation ranges are on the order of 2π rad (~13 ms at 75 Hz) but the pulse time spread is much smaller and is of order 0- 5 ms

rms. In terms of scintillations, the PDF of peak intensity is very nearly lognormal and for the peak $\sigma^2_{\ln I} \approx 0.5$, which is close to, but in excess of, the weak fluctuation limit of 0.3. The value of $\sigma^2_{\ln I}$ is also much less than the fully saturated value of 1.64. Further, predictions of the pulse time spread from the path integral theory (not discussed here) are typically 500 ms [Colosi et al., 1999a; Dashen et al., 1985]; two orders of magnitude too large! Collectively these observations show behaviour more typical of the unsaturated or nearly partially saturated regime.

On the other hand, $\sigma^2_{\ln I}$ is a strong function of time delay relative to the peak. At the peak, $\sigma^2_{\ln I}$ attains its minimum value, but nearly triples at a time delay +/- 30 ms away from the peak. Further, there is significant wavefront fracturing which creates more than one peak along the wavefront. It is found that on average there are roughly 2 peaks per wavefront segment per hydrophone depth. These qualities are more indicative of the partially saturated regime.

3.2.2 The finale region

Figure 3 shows that all rays are predicted to be in the fully saturated regime, and that there is no indication of a rapid transition between the wavefront region and the finale region. Further, as figure 1 shows, there is significant scattering of energy into the predicted shadow zone between travel times of 2196 (s) and 2197 (s); in this region the assumption of an unperturbed ray (as in Eq. 1,2,4, and 5) is grossly violated. Because of these issues, one must regard the agreement between the Λ,Φ theory prediction and the observation of saturated statistics as purely fortuitous. The observations in the finale are discussed in detail in Colosi, Tappert, and Dzieciuch, [2001] who find that the PDF of intensity is very nearly exponential with $\sigma^2_{\ln I} \cong \pi^2/6$.

4. NEW THEORETICAL APPROACHES

Clearly the results of the previous section show serious shortcomings in the Λ,Φ theory, and the path integral theory for pulse time spread, when these theories are applied to very long transmission ranges. These theories have enjoyed relative success for ranges up to a few hundred km (but more typically tens of km) and frequencies from a few hundred Hz to a few kHz. A new approach is needed to interpret long-range data, and perhaps also to re-interpret shorter range data!

I examine two very different viewpoints. One is ray based and relies on the physical intuition one obtains from ray methods. The obvious analogy here is to the problem of the rainbow. Partial wave expansions of the rainbow light field while constituting a full solution to the problem are not physically illuminating. But when ray methods are applied to the problem, they describe many of the rainbow features like the primary and secondary bow angles, the reversal of color ordering in the primary and secondary bows, and the polarization of the rainbow. In addition ray methods show that the rainbow is a caustic and that a detailed description of the intensity will require full wave, diffraction effects.

The second approach I will examine goes back to full wave methods and treats the signal bandwidth in a rigorous way. The ATOC basin scale transmissions were very broadband, with a

center frequency of 75 Hz and a bandwidth of 37.5 Hz (roughly a Q of 2). Here we are limited to perturbation methods and the Born approximation is employed, which transforms the stochastic problem from one of multiplicative noise, which is very hard to solve, to one of additive noise which is much easier to solve. This approach is enlightening because it has the Λ,Φ theory as a limiting case; i.e. zero bandwidth.

The ray chaos problem in underwater acoustics has been discussed by many investigators [Smith, Brown and Tappert, 1992a,b; Simmen, Flatt'e and Wang, 1997, Wolfson and Tappert, 2000 and Wolfson and Tomsovic, 2001], but none of the published work to date has dealt with realistic ocean environments. Therefore the following discussion is rather new. The question of broadband scattering goes back to the 1950's, but the particular treatment in terms of the Born approximation is discussed in detail only recently by Colosi, 1999a. The following discussion of broadband scattering is largely a review of this work.

4.1 Ray Chaos

It is well established that ray trajectories in the ocean sound channel are governed by a set of nonlinear equations which in the case of range dependent sound speed structure can show exponential sensitivity to initial conditions or chaotic behaviour. This nonlinearity is most easily demonstrated using the parabolic approximation to the wave equation,

$$\frac{i}{k}\frac{\partial\psi}{\partial x} = -\frac{1}{2k^2}\frac{\partial^2\psi}{\partial z^2} + U(z,x)\psi \qquad (6)$$

where $k = \omega/c_0$, $c(z,x) = c_0(1+U(z,x))$, and ω is the wave frequency. The Euler-Lagrange equation for the raypath $z_r(x)$ in the parabolic approximation is,

$$\frac{d^2 z_r}{dx^2} + \frac{\partial U}{\partial z} = 0 \qquad (7)$$

where it should be noted that even for range independent ocean sound speed profiles (c=c(z), and ignoring unrealistic linear and quadratic profiles) Eq. 7 is nonlinear.

4.1.1 Hamiltonian form

The ray equations can be written in Hamiltonian form, and for the Helmholtz equation the form of the Hamiltonian is,

$$H(z,p;x) = -\left(c^{-2} - p^2\right)^{1/2} \qquad (8)$$

where the canonically conjugate variables are the ray slowness $p = \sin(\theta)/c$, and the ray depth, z. Hamilton's equations are,

$$\dot{z} = \frac{dz}{dx} = \frac{\partial H}{\partial p} \qquad (9)$$

$$\dot{p} = \frac{dp}{dx} = -\frac{\partial H}{\partial z} \qquad (10)$$

with the supplemental travel time equation,

$$\dot{T} = \frac{dT}{dx} = \frac{1}{H c^2}. \qquad (11)$$

The notion of ray chaos arises if there is "no constant of the motion", χ, such that,

$$\frac{d\chi}{dx} = \frac{\partial \chi}{\partial z}\frac{dz}{dx} + \frac{\partial \chi}{\partial p}\frac{dp}{dx} + \frac{\partial \chi}{\partial x} = 0 \qquad (12)$$

For c=c(z) the Hamiltonian, H, is a constant of the motion and all rays are non-chaotic. For a general c=c(z,x), like our random medium problem of propagation through stochastic internal waves, my experience shows that all the rays are chaotic.

4.1.2 Qualitative comparisons with observations

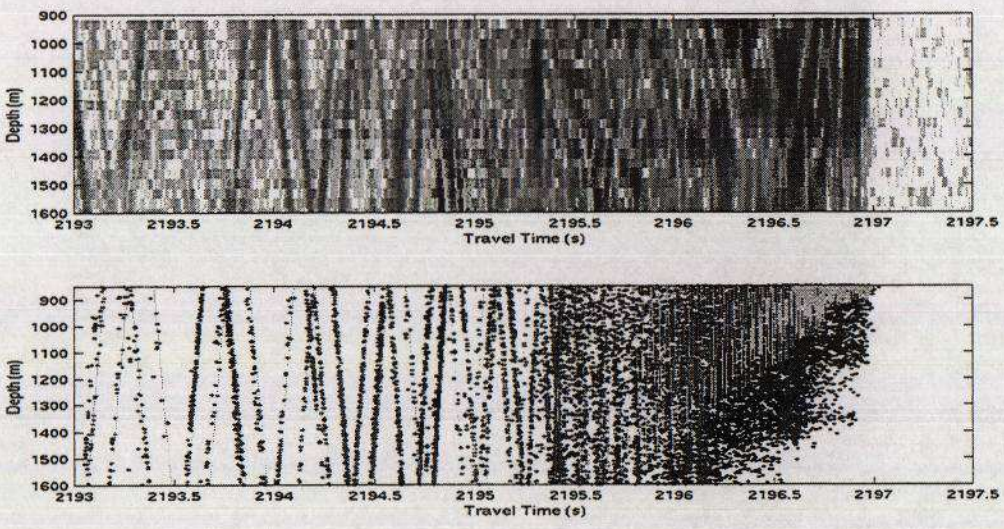

Figure 4: A measured pulse from a 3252km transmission (upper) and ray simulation calculations with (dots) and without (grey-lines) internal waves (lower).

I have computed ray paths and travel times for 3252km propagation through GM internal waves superimposed on background sound speed fields derived from climatology and XBT data [Colosi et al., 1999, and Worcester et al., 1999]. In figure 4 below a comparison is made between an observed pulse and the ray simulations with and without internal waves. Qualitatively, the comparison is quite good. In the wavefront region the simulations and the data both show clear wavefront sections, but only the simulation with internal waves shows the distinct fracturing of the

wavefront as is seen in the observations. Further, in the ray simulation with internal waves a rapid transition is clear from the wavefront region into the finale region, and the scattering of energy into the shadow zone between times 2196 and 2197 (s) is also consistent with the observations. Finally, the ray simulation in the finale shows the field to be a complex interference pattern of many closely spaced and phase randomised rays, thus supporting the notion of a fully saturated propagation regime (as observed).

To examine the transition between wavefronts and finale further, we compute the exponential growth rates of the ray instabilities from the ray simulations; these are called the Lyapunov exponents, υ [Tabor, 1987], and there is a particular value of υ for each initial value of momentum p, and for several realizations of the internal wave field. In the absence of internal waves υ is very small or zero. Figure 5 shows values of υ computed from our simulation as a function of travel time. In all cases, υ is significantly different from zero and the spread in values of υ is due to the different realizations of the internal wave field (Wolfson and Tomsovic, 2001 show that the PDF of υ is very closely normal with variance which decreases in range as 1/R). For rays in the wavefront region, the typical value of υ is about 1/200km whereas in the finale region, a typical number is about 1/40km. This is a large difference, especially when one considers these are exponential growth rates. The rapid transition from finale to wavefront region is captured in figure 5.

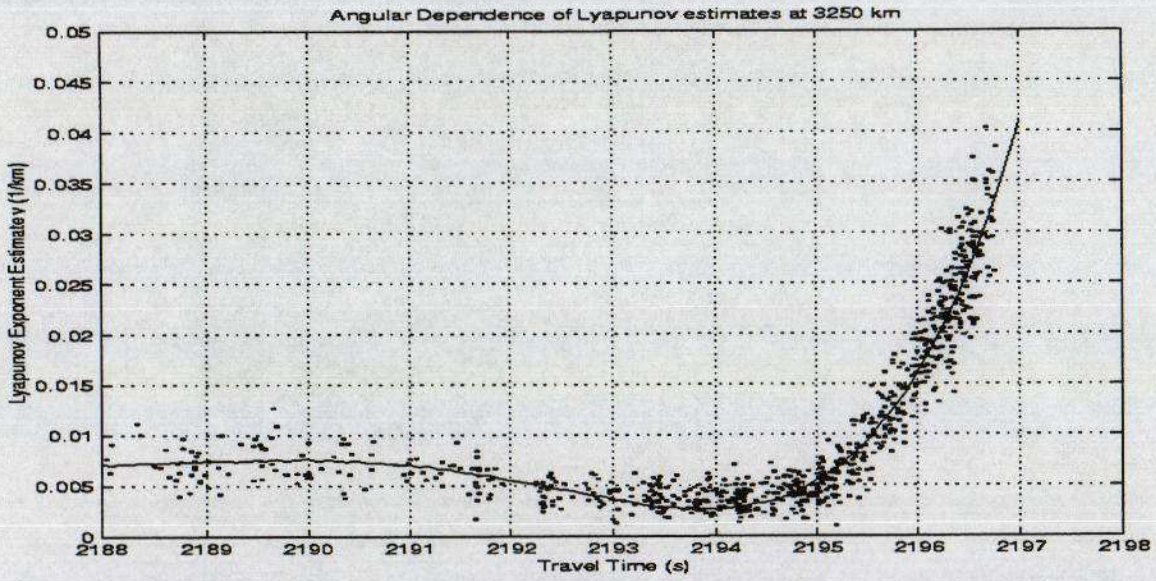

Figure 5: Angular dependence of the stability exponent (Lyapunov exponent) here plotted as a function of ray travel time. The high angle rays with early travel times (wavefront region) are much more stable than the low angle rays with late travel times (finale region). The computed transition time at 2195 (s) is quite abrupt and is in good agreement with the observations.

Clearly there are some very interesting and tantalizing comparisons to the observations, and more work will be needed to understand the ray results. Some interesting questions are:

1) What factors determine the transition region between the wavefront and finale regions?
2) Why is the stable wavefront pattern seen in the ray simulations, despite the fact that the 3252 km range is more than 15 e-folding lengths?

4.1.3 Stochastic ray tubes

The rays simulations thus presented show that in the wavefront region there is not one eigenray connecting a given receiver depth and wavefront arm but many. Figure 6 shows an expanded view of one of the wavefront arms, and the multiple eigenray contributions are quite evident. The multiple eigenrays all arrive very close in travel time to the unperturbed ray; the time spread is roughly +/- 10 ms (close to the observed value!). Figure 6 also shows the phase space (p,z) for this wavefront arm which reveals the stretched and folded structure typical of chaotic systems. This stretching and folding gives rise to many caustics which can be identified by the condition $dz/d\,p_0 = 0$ (i.e. tangent points along the (p,z) curve). Because of the large number of caustics revealed by the ray calculation one must be very careful in using ray ideas to describe intensity behaviour. Ray theory fails near caustics, and this is an example (as in the rainbow problem) how ray theory can alert us to problems which require full wave treatment.

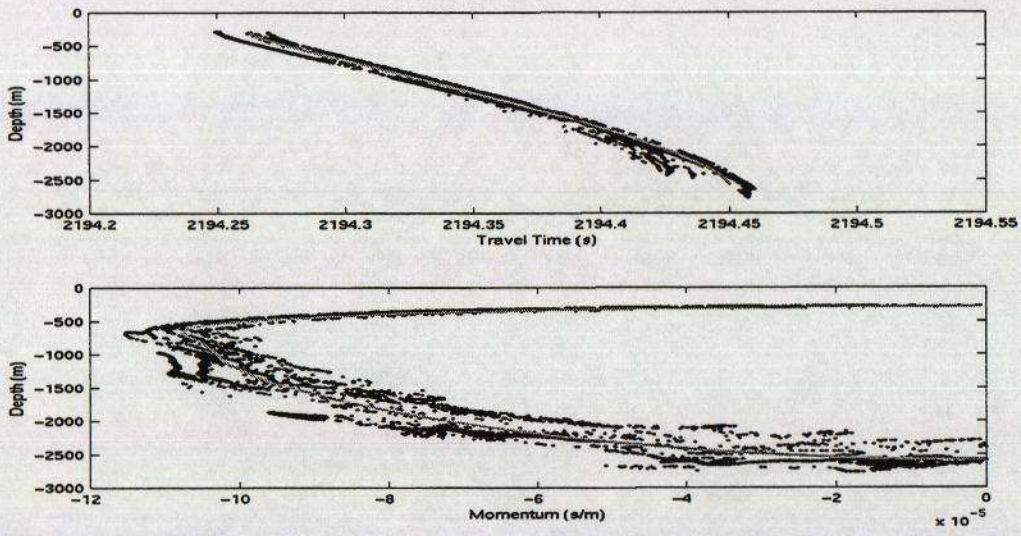

Figure 6: Expanded view of a wavefront arm in time-depth space (upper) and in phase space (p,z;lower). Black dots are the internal wave simulation and the thick grey line is the simulation without internal waves.

In figure 6 it was shown that the multiple eigenray contributions are very close in travel time to the unperturbed ray, but what about the spatial behaviour? Figure 7 is a plot of the stochastic eigenray ray paths which reach a particular wavefront arm and receiver depth. In this case there were over 400 eigenrays found! Also plotted in figure 7 is the unpertubed ray path (Gray). We can see that the stochastic eigenrays broadly fill the ocean, particularly in the middle of the propagation path (middle panel). It has been found that the stochastic eigenrays with the highest intensity are not necessarily close to the unperturbed ray and may infact be found anywhere within the stochastic ray bundle. We term this phenomenon "stochastic ray tubes" and there are potentially some serious implications of this phenomenon to ocean acoustic tomography. In particular, tomography relies on knowing the spatial sampling properties of the ray to obtain vertical resolution. These calculations imply that this vertical information is smeared out over

perhaps 100m. The horizontal smearing is not so important since there is essentially no horizontal resolution even in a non-fluctuating ocean. Finally there is an additional interesting result that comes out of these calculations, namely that the total number of upper and lower turning points (wavefront ID) of the stochastic eigenrays is exactly the same as the ID for the unperturbed ray! This means that, while the internal waves broaden or blur the ray tube, they do not completely destroy one of its basic characters; the identification (or ID).

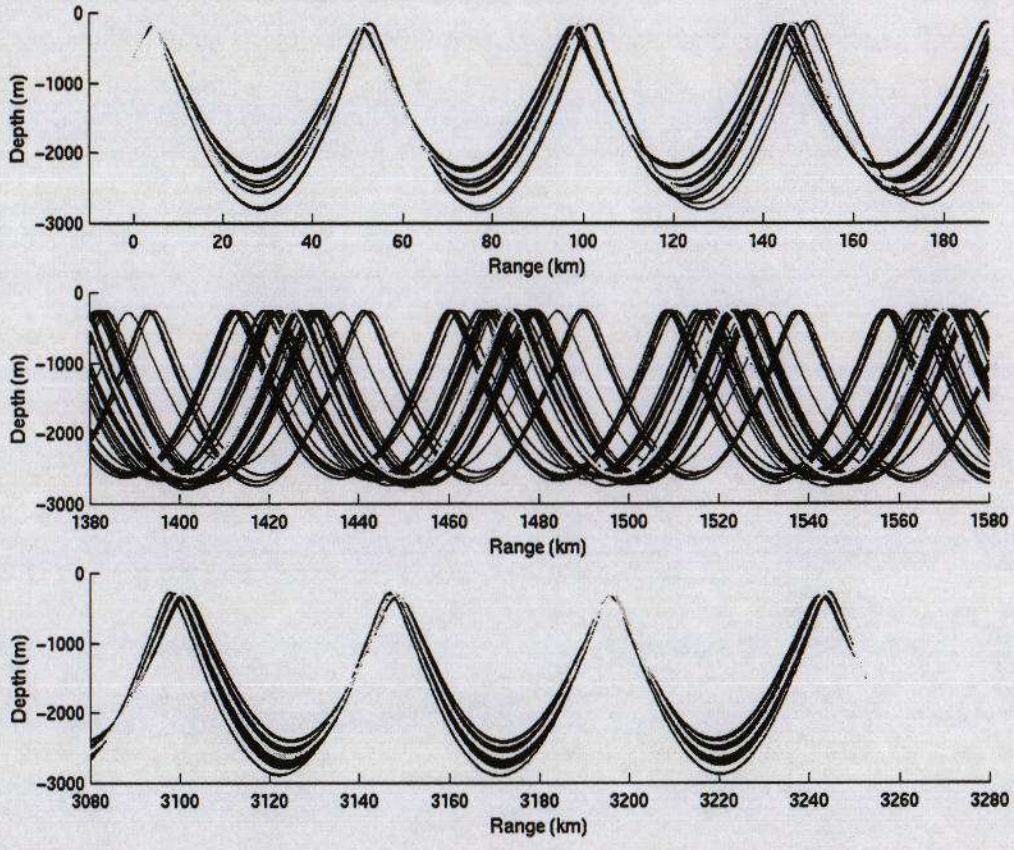

Figure 7: Stochastic ray tubes for 3250-km propagtion through GM internal waves at half the reference energy. The unpertubed ray path (thick grey curves) and over 400 stochastic eigenrays (thin black curves) are plotted for the beginning, middle, and end (upper/middle/lower) of the propagation path. The receiver depth is at 1500m and the wavefront ID is 137.

4.2 Broadband Scattering: Born Theory

The ray calculations and the chaos based interpretations presented in the previous section are compelling, but there are significant issues with the neglect of diffraction effects, particularly since

so many caustics are predicted by the ray theory; on any place in the wavefront, one is always close to several caustics regardless of whether the wavefront or finale regions are considered. Therefore, I address another issue in waves in random media, namely broadband pulse propagation. The treatment here is based on Colosi, 1999b, and is really just a toy model which is intended to underline the differences between broadband and narrowband scattering. The method I am going to discuss is based on the Born approximation, which is a weak scattering approximation and would not be expected to work at basin scale ranges. Note that the Rytov approximation, which is the basis of the Λ,Φ theory, is also a weak scattering theory (the Rytov and Born approximations are very closely related). I have not shown it explicitly, but I conjecture that my broadband Born theory does have the Λ,Φ theory as a limiting case where the bandwidth goes to zero.

The essence of the broadband Born theory is actually quite simple, but the details are somewhat cumbersome (the reader is referred to Colosi 1999b for the details). For simplicity I assume a constant background sound speed and a Gaussian wave packet. Then using the first Born series approximation, an expression for the time-domain signal is obtained in the form,

$$\Psi(\vec{r},t) = \Psi_0(\vec{r},t)(1+\varphi_1(\vec{r},t)) \qquad (13)$$

where Ψ_0 is the unperturbed wavepacket, and φ_1 is the scattered field which depends on the center frequency ω_c, the Fresnel radius $R_f^2(x) = \lambda x(R-x)/R$, and the ratio of bandwidth to center frequency, $q = \Delta\omega/\omega_c$. Because of the form of Eq. 13 (it looks like the first 2 terms in a Taylor expansion of the exponential), we can associate the $2\mathrm{Re}[\varphi_1]$ with variations in the log-intensity of the signal, and $\mathrm{Im}[\varphi_1]$ with variations in the signal phase. Using these ideas the variances of log-intensity, $\sigma^2_{\ln I}$ and phase, $\langle\phi^2\rangle$ can be be written as volume integrals of the fractional sound speed correlation function, $\langle\mu(r_1)\mu(r_2)\rangle$ times a weighting function,

$$\sigma^2_{\ln I} = 4k_c^2\int_V d^3r_1\int_V d^3r_2 W_\chi(r_1)W_\chi(r_2)\langle\mu(r_1)\mu(r_2)\rangle \qquad (14)$$

$$\langle\phi^2\rangle = k_c^2\int_V d^3r_1\int_V d^3r_2 W_\phi(r_1)W_\phi(r_2)\langle\mu(r_1)\mu(r_2)\rangle \qquad (15)$$

where k_c is the center frequency wavenumber and W_χ and W_ϕ are the log-amplitude and phase weighting functions. The weighting functions are complicated functions which depend on the center frequency, Fresnel radius, q, and the time delay τ relative to the unperturbed pulse peak. Figure 8 shows a plot of the weighting functions using the ATOC center frequency and bandwidth for $\tau = 0$. For a single frequency, it is well known that phase is most sensitive to the largest scales in the problem and log-intensity is most sensitive to scales near the Fresnel radius. However, it is seen that the broadband weighting function is much more concenetrated around the unperturbed ray path (i.e. $Y^2 + Z^2 = 0$) and the weighting properties are much different from the

single frequency case; all the effect is concentrated within a single Fresnel zone. Though these cases are not shown here, the weighting functions are also a strong function of the time delay τ (see Colosi, 1999b). For $\tau > 0$ on the rise of the pulse (early travel times relative to the peak) the weighing functions are strongly concentrated around the unperturbed ray and for $\tau < 0$ (late travel times relative to the peak) contributions start coming in from locations much further away from the ray which naturally have longer travel times.

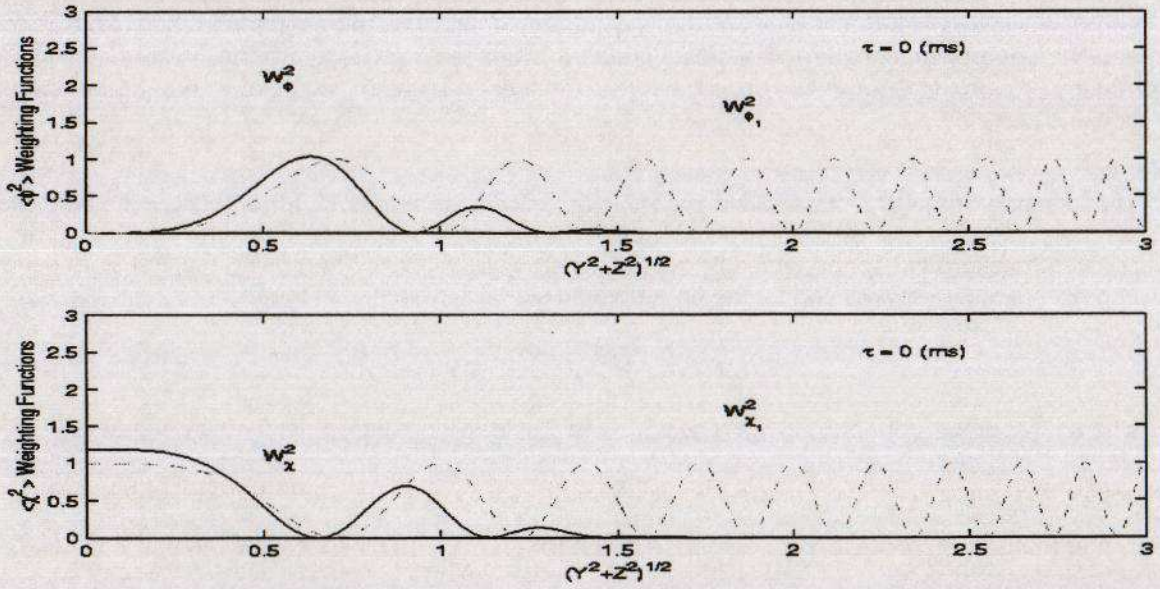

Figure 8: Broadband (Solid) and single frequency (Dash) weighting functions for log-amplitude (lower) and phase (upper) for a time delay, τ=0 relative to the unperturbed peak arrival time. The bandwidth and center frequency were chosen to be consistent with the ATOC signal. The horizontal axis is radial distance from the straight-line ray measured in Fresnel radii.

The inescapable conclusion here is that pulse propagation is quite different from the single frequency cases for which the Λ,Φ theory is derived. This area, like ray chaos, presents an exciting new frontier in ocean acoustic wave propagation through random media, where I hope there will be significant progress in the coming years.

4.3 Beyond internal waves and GM

Finally a few brief words must be said concerning the random medium itself; i.e the ocean. In the 1970's the introduction of the Garrett-Munk (GM) internal wave spectrum to the problem of ocean acoustic wave propagation was a significant breakthrough, as all previous work in the area had misguidedly attempted to graft the atmospheric theory of homogeneous isotropic fluctuations onto the ocean problem. The ocean sound speed fluctuations are neither homogeneous nor isotropic.

For basin scale acoustic propagation, several considerations demand that we go beyond GM internal waves. First, basin scales transmission ranges involve many correlation lengths of the ocean mesoscale field, whose characteristic scale is the first mode Rossby deformation radius [Pedlosky, 1980], of order 50km in the temperate latitude open ocean. A typical temperature anomaly for an eddy is 1 °C (or roughly 5 m/s sound speed). Therefore the horizontal gradients of eddies are roughly the same as internal waves, which have characteristic horizontal scale of

10km and temperature anomalies of roughly 0.2 °C . There does exist a reasonable model for the open ocean eddy field which is based on satellite altimetry data from the Topex/ Poseidon spacecraft [Stammer, 1994].

The second feature of basin scale transmission that leads us away from GM is that the sound has significant upper ocean interaction. The GM model was based largely on measurements within or below the main thermocline (roughly 1500 to 400m depth at temperate latitudes) . In the upper ocean, several different mechanisms can contribute to sound speed variability. Examples are:

1) Wind forced inertial oscillations (which have large shear!)
2) Millifronts (small scale fronts of internal wave scale) caused by ocean stirring (Dzieciuch , Munk, and Remmich)
3) Thinning of the internal wave guide (IW mode turning points)
4) Variable mixed layer depth

Recent calculations by Dzieciuch and Munk (personal communication) suggest that millifront scattering in the upper ocean can be at-least as strong as upper ocean internal wave scattering. Further calculations of Colosi (personal communication) show that in the eastern North Pacific (a very quiet mesoscale region) mesoscale contributions to horizontal coherence can be just as important as GM internal wave contributions. However the general state of affairs is that many of these processes have not been explored in any detail, so there are some very interesting new oceanographic as well as acoustics problems that can be considered for basin scales.

5. SUMMARY

Based largely on observations in the 1990's, the view of basin scale wave propagation through random media, and perhaps the overall field of ocean random media, is quite different now. We are looking at new theoretical methods which include dynamical systems theory related to rays and broadband theory which may provide an extension to the Λ,Φ theory. Further there is a significant need to explore new ocean processes as sources of acoustic variability. While the state of affairs in basin scale acoustics is disorderly, this uncertainty provides fertile ground for new discovery. This is the situation in which A.B. Wood often found himself and invariably he built-up a new field of study based on first principles, some data, and great intuition. It is this uncertainty and the quest for resolutions that makes science exciting and if we could ask A. B. Wood I think he would agree.

6. ACKNOWLEDGEMENTS

The author is indebted to the Walter Munk, Peter Worcester, Matthew Dzieciuch, Bruce Cornuelle, Bruce Howe, James Mercer, Bob Spindel, Kurt Metzgar, Ted Birdsall and Art Baggeroer for the design of the experimental equipment and the collection of the basin scale acoustic and oceanographic data under unusually difficult circumstances. I am also grateful to Mike Brown, Fred Tappert, Mike Wolfson, Frank Henyey, and Steven Tomsovic whose work is the source of much of the information in the ray chaos section. Finally I am very grateful to Jim Lynch for reading over this paper and providing some excellent editorial comments.

REFERENCES

[1] Au, W.W.L., P.E. Nachtigall, and J.L. Pawlowski, Acoustic effects of the ATOC signal (75Hz, 195dB) on dolphins and whales, J. Acoust. Soc. Am. 1997; 101: 2973-77

[2] Colosi, J.A. and M.G. Brown, Efficient numerical simulation of stochastic internal wave induced sound speed perturbation fields, J. Acoust. Soc. Am. 1998; 103, 2232-35

[3] Colosi, J.A. and the ATOC Group, Comparisons of measured and predicted acoustic fluctuations for a 3252-km propagation experiment in the eastern North Pacific Ocean, J. Acoust. Soc. Am. 1999; 105: 3202-18.

[4] Colosi, J.A. and the ATOC Group, A review of recent results on ocean acoustic wave propagation in random media: basin scales, IEEE J. Oc. Eng. 1999; 24: 138-55

[5] Colosi, J.A., F. Tappert, and M. Dzieciuch, Further analysis of intensity fluctuations for a 3252-km acoustic propagation experiment in the eastern North Pacific Ocean, J. Acoust. Soc. Am. 2001,

[6] Costa, D.P., D.E. Crocker, D.M. Waples, P.M. Webb, J. Gedamke, D. Houser, P.D. Goley, B.J. LeBoeuf, and J. Calambokidis, The California Marine Mammal Research Program for the Acoustic Thermometry of Ocean Climate experiment, In: Conference Proceedings of California and the World Ocean 1997: Taking a look at California's ocean resources: an agenda for the future, O.T. Magoon et al. (eds), American Society of Civil Engineers, Reston VA: 1542-53

[7] Dashen, R., S.M. Flatt'e, and S. Reynolds, Path-integral treatment of acoustic mutual coherence functions for rays in the sound channel, J. Acoust. Soc. Am. 1985; 77: 1716-22

[8] Dushaw, B.D., B.M. Howe, J.A. Mercer, R.C. Spindel, and the ATOC Group, Multimegameter-Range acoustic data obtained by bottom-mounted hydrophone arrays for measurement of ocean temperature, IEEE J. Oc. Eng. 1999; 24: 202-14

[9] Esswein, R. and S.M. Flatt'e, Calculation of the phase-structure function density for oceanic internal waves, J. Acoust. Soc. Am. 1981; 70: 1387-96

[10] Flatt'e S.M., R. Dashen, W. Munk, K. Watson, and F. Zachariason, *Sound Transmission through a fluctuating ocean*, Cambridge University Press, Cambridge, 1979

[11] Flatt'e, S.M., Wave propagation through random media: Contributions from ocean acoustics, Proc. IEEE 1983; 71: 1267-94

[12] Frankel, A.S., and C.W. Clark, Results of low-frequency playback of M-sequence noise to humpback whales, Megaptera novaeangkiae, in Hawai'I, Can. Jour. Zool., 1998; 76: 521-35

[13] Frankel, A.S., and C.W. Clark, Behavioral responses of humpback whales (Megaptera novaeanliae) to full-scale ATOC signals, J. Acoust. Soc. Am., 2000; 108: 1930-37

[14] Klimey, A.P. and S.C. Beavers, Playback of acoustic thermometry of ocean climate (ATOC) – like signals to bony fishes to evaluate phonotaxis, J. Acoust. Soc. Am., 1998; 104: 2506-10

[15] Munk, W., Internal waves and small scale processes, in The Evolution of Physical Oceanography, eds B. Warren and C. Wunsch 1981: 264-91

[16] Munk, W., Worcester, P., and Wunsch, C., *Ocean Acoustic Tomography*, Cambridge University Press, Cambridge, 1995

[17] Munk, W. and A.M.G. Forbes, Global Warming: an acoustic measure?. J. Phys. Oc. 1989; 19: 1765-78

[18] Pedlosky, J, *Geophysical Fluid dynamics*, Springer-Verlag, New York, 1987.

[19] Simmen, J., S.M. Flatt'e, and G. Wang, Wavefront folding, chaos, and diffraction for sound propagation through ocean internal waves, J. Acoust. Soc. Am. 1997; 102: 239-55

[20] Spiesberger, J.L. and K. Metzger Jr., Basin-scale tomography: a new tool for studying weather and climate, J. Geophys. Res. 1991; 96: 4869-89

[21] Semtner, A.J. and R.M. Chervin, Environmental effects on acoustic measures of global warming J. Geophys. Res. 1990; 95: 12973-82

[22] Smith, K.B., M.G. Brown, and F.D. Tappert, Ray chaos in underwater acoustics, J. Acoust. Soc. Am. 1992; 91: 1939-49

[23] Smith, K.B., M.G. Brown, and F.D. Tappert, Acoustic ray chaos induced by mesoscale ocean structure, J. Acoust. Soc. Am. 1992; 91: 1950-59

[24] Stammer, D, Global characteristics of ocean variability estimated from regional TOPEX/POSEIDON altimeter measurements, J. Phys. Oc., 1996; 101: 25779-811

[25] Tabor, M., *Chaos and integrability in nonlinear dynamics*, Wiley-Interscience Publications, New York, 1989

[26] The ATOC group, Ocean Climate Change: Comparisons of acoustic tomography, satellite altimetry, and modelling, Science 1998; 281: 1327-32.

[27] Wolfson, M.A., and F.D. Tappert, Study of horizontal multipaths and ray chaos due to ocean mesoscale structure, J. Acoust. Soc. Am. 2000; 107: 154-62

[28] Wolfson, M.A., and S. Tomsovic, On the stability of long-range sound propagation through a structured ocean, J. Acoust. Soc. Am. 2001,

[29] Worcester, P.F. and the ATOC group, A test of basin scale acoustic thermometry using a large aperture vertical array at 3252-km range in the eastern North Pacific Ocean, J. Acoust. Soc. Am. 1999; 105: 3185-3201